

## Chemically Self-Consistent Modeling of the Globular Cluster NGC 2808 and its Effects on the Inferred Helium abundance of Multiple Stellar Populations.

2 EMILY M. BOUDREAU<sup>1</sup>, BRIAN C. CHABOYER<sup>1</sup>, AMANDA ASH<sup>2</sup>, RENATA EDAES HOH<sup>1</sup>, AND GREGORY FEIDEN<sup>2</sup>

3 <sup>1</sup>*Department of Physics and Astronomy, Dartmouth College, Hanover, NH 03755, USA*

4 <sup>2</sup>*Department of Physics and Astronomy, University of North Georgia, Dahlonega, GA 30533, USA*

### 5 ABSTRACT

6 The Helium abundances in the multiple populations which are now known to comprise all closely  
7 studied Milky Way globular clusters are often inferred by fitting isochrones generated from stellar  
8 evolutionary models to globular cluster photometry. It is therefore important to build stellar models  
9 that are chemically self-consistent in terms of their structure, atmosphere, and opacity. In this work  
10 we present the first chemically self-consistent stellar models of the Milky Way Globular Cluster NGC  
11 2808 using MARCS model atmospheres, OPLIB high-temperature radiative opacities, and AESOPUS  
12 low-temperature radiative opacities. These stellar models were fit to the NGC 2808 photometry using  
13 *Fidanka*, a new software tool that was developed optimally fit cluster photometry to isochrones and  
14 for population synthesis. *Fidanka* can determine, in a relatively unbiased way, the ideal number of  
15 distinct populations which exist within a dataset and then fits isochrones to each population. We  
16 achieve this through a combination of Bayesian Gaussian Mixture Modeling and a novel number  
17 density estimation algorithm. Using *Fidanka* and F275W-F814W photometry from the Hubble UV  
18 Globular Cluster Survey we find that the helium abundance of the second generation of stars in NGC  
19 2808 is higher than the first generation by  $15 \pm 3\%$ . This is in agreement with previous studies  
20 of NGC 2808. **This work, along with previous work by Dotter et al. (2015) focused on  
21 NGC 6752 demonstrates that chemically self-consistent models of globular clusters do  
22 not significantly alter inferred helium abundances and are therefore unlikely to be worth  
23 the significant additional time investment.**

24 *Keywords:* Globular Clusters (656), Stellar evolutionary models (2046)

### 25 1. INTRODUCTION

26 Globular clusters (GCs) are among the oldest observ-  
27 able objects in the universe (Peng et al. 2011). They  
28 are characterized by high densities with typical half-  
29 light radii of  $\leq 10$  pc (van den Bergh 2010), and typi-  
30 cal masses ranging from  $10^4$ – $10^5 M_{\odot}$  (Brodie & Strader  
31 2006) — though some GCs are significantly larger than  
32 these typical values (e.g.  $\omega$  Cen, Richer et al. 1991).  
33 GCs provide a unique way to probe stellar evolution  
34 (Kalirai & Richer 2010), galaxy formation models  
35 (Boylan-Kolchin 2018; Kravtsov & Gnedin 2005), and  
36 dark matter halo structure (Hudson & Robison 2018).

37 The traditional view of Globular Clusters was that  
38 they consisted of a single stellar population (SSP, in  
39 some publications this is referred to as a Simple Stel-  
40 lar Population). This view was supported by spectro-  
41 scopically uniform heavy element abundances (Carretta  
42 et al. 2010; Bastian & Lardo 2018) across most clus-  
43 ters (M54 and  $\omega$  Cen are notable exceptions, see Marino  
44 et al. (2015) for further details), and the lack of ev-  
45 idence for multiple stellar populations (MPs) in past  
46 color-magnitude diagrams of GCs (i.e. Sandage 1953;  
47 Alcaino 1975). However, over the last 40 years non-  
48 trivial star-to-star light-element abundance variations  
49 have been observed (i.e. Smith 1987) and, in the last  
50 two decades, it has been definitively shown that most if  
51 not all Milky Way GCs have MPs (Gratton et al. 2004,  
52 2012; Piotto et al. 2015). The lack of photometric evi-  
53 dence for MPs prior to the 2000, can be attributed to the

54 more narrow color bands available, until very recently, to  
55 ground based photometric surveys (Milone et al. 2017).

56 The prevalence of multiple populations in GCs is so  
57 distinct that the proposed definitions for what consti-  
58 tutes a globular cluster now often center the existence  
59 of MPs (e.g. Carretta et al. 2010). Whereas, people have  
60 have often tried to categorized objects as GCs through  
61 relations between half-light radius, density, and surface  
62 brightness profile, in fact many objects which are gener-  
63 ally thought of as GCs don't cleanly fit into these cuts  
64 (Peebles & Dicke 1968; Brown et al. 1991, 1995; Bekki  
65 & Chiba 2002). Consequently, Carretta et al. (2010)  
66 proposed a definition of GC based on observed chem-  
67 ical inhomogeneities in their stellar populations. The  
68 modern understanding of GCs then is not simply one of  
69 a dense cluster of stars that may have chemical inho-  
70 mogeneities and multiple populations; rather, it is one  
71 where those chemical inhomogeneities and multiple pop-  
72 ulations themselves are the defining element of a GC.

73 All Milky Way globular clusters studied in detail show  
74 populations enriched in He, N, and Na while also be-  
75 ing deplete in O and C (Piotto et al. 2015; Bastian &  
76 Lardo 2018). **Further, studies of Magellenic Cloud**  
77 **massive clusters have shown that these light el-**  
78 **ement abundance variations exist in clusters as**  
79 **young as  $\sim 2$  Gyr but not in younger clusters**  
80 **(Martocchia et al. 2019) while there is also evi-**  
81 **dence of nitrogen variability in the  $\sim 1.5$  Gyr old**  
82 **cluster NGC 1783 (Cadelano et al. 2022).** These  
83 light element abundance patterns also are not strongly  
84 correlated with variations in heavy element abundance,  
85 resulting in spectroscopically uniform Fe abundances be-  
86 tween populations (**though recent work indicates**  
87 **that there may be [Fe/H] variations within the**  
88 **first population, e.g. Legnardi et al. 2022; Lardo**  
89 **et al. 2022)**. Further, high-resolution spectral studies  
90 reveal anti-correlations between N-C abundances, Na-O  
91 abundances, and potentially Al-Mg (Snedden et al. 1992;  
92 Gratton et al. 2012). Typical stellar fusion reactions  
93 can deplete core oxygen; however, the observed abun-  
94 dances of Na, Al, and Mg cannot be explained by the  
95 CNO cycle (Prantzos et al. 2007). Consequently, glob-  
96 ular cluster populations must be formed by some novel  
97 means.

98 Formation channels for these multiple populations re-  
99 main a point of debate among astronomers. Most pro-  
100 posed formation channels consist of some older, more  
101 massive, population of stars polluting the pristine clus-  
102 ter media before a second population forms, now en-  
103 riched in heavier elements which they themselves could  
104 not have generated (for a detailed review see Gratton  
105 et al. 2012). The four primary candidates for these pol-

106 luters are asymptotic giant branch stars (AGBs, Ventura  
107 et al. 2001; D'Ercole et al. 2010), fast rotating mas-  
108 sive stars (FRMSs, Decressin et al. 2007), super mas-  
109 sive stars (SMSs, Denissenkov & Hartwick 2014), and  
110 massive interacting binaries (MIBs, de Mink et al. 2009;  
111 Bastian & Lardo 2018).

112 Hot hydrogen burning (i.e. proton capture), material  
113 transport to the surface, and material ejection into the  
114 intra-cluster media are features of each of these models  
115 and consequently they can all be made to *qualitatively*  
116 agree with the observed elemental abundances. How-  
117 ever, none of the standard models can currently account  
118 for all specific abundances (Gratton et al. 2012). AGB  
119 and FRMS models are the most promising; however,  
120 both models have difficulty reproducing severe O deple-  
121 tion (Ventura & D'Antona 2009; Decressin et al. 2007).  
122 Moreover, AGB and FRMS models require significant  
123 mass loss ( $\sim 90\%$ ) between cluster formation and the  
124 current epoch — implying that a significant fraction of  
125 halo stars formed in GCs (Renzini 2008; D'Ercole et al.  
126 2008; Bastian & Lardo 2015).

127 In addition to the light-element anti-correlations ob-  
128 served, it is also known that second populations are sig-  
129 nificantly enhanced in Helium (Piotto et al. 2007, 2015;  
130 Latour et al. 2019). Depending on the cluster, helium  
131 mass fractions as high as  $Y = 0.4$  have been inferred (e.g.  
132 Milone et al. 2015a). However, due to both the relatively  
133 high and tight temperature range of partial ionization  
134 for He and the efficiency of gravitational settling in core  
135 helium burning stars, the initial He abundance of glob-  
136 ular cluster stars cannot be observed; consequently, the  
137 evidence for enhanced He in GCs originates from com-  
138 parison of theoretical stellar isochrones to the observed  
139 color-magnitude-diagrams of globular clusters. There-  
140 fore, a careful handling of chemistry is essential when  
141 modeling with the aim of discriminating between MPs;  
142 yet, only a very limited number of GCs have been stud-  
143 ied with chemically self-consistent (structure and atmo-  
144 sphere) isochrones (e.g. Dotter et al. 2015, NGC 6752).

145 NGC 2808 is the prototype globular cluster to host  
146 Multiple Populations. Various studies since 2007 have  
147 identified that it may host anywhere from 2-5 stellar  
148 populations. These populations have been identified  
149 both spectroscopically (i.e. Carretta et al. 2004; Carretta  
150 2006; Carretta et al. 2010; Gratton et al. 2011; Carretta  
151 2015; Hong et al. 2021) and photometrically (i.e. Piotto  
152 et al. 2007, 2015; Milone et al. 2015a, 2017; Pasquato &  
153 Milone 2019). Note that recent work (Valle et al. 2022)  
154 calls into question the statistical significance of the de-  
155 tectations of more than 2 populations in the spectroscopic  
156 data. Here we present **the first stellar structure and**

157 **evolutionary models built in a chemically self-**  
 158 **consistent manner of NGC 2808.**

159 We model the photometry of the **primordial pop-**  
 160 **ulation (hereafter P1) and the helium enriched**  
 161 **population (hereafter P2). Milone et al. (2015a)**  
 162 **identifies 5 populations within NGC 2808, given**  
 163 **that the aim of this work is not to identify sub-**  
 164 **populations; rather, to measure the effect that**  
 165 **chemical self consistent stellar structure and evo-**  
 166 **lutionary have on the inferred helium abundance**  
 167 **for the two most extreme cases, we do not con-**  
 168 **sider more than those two populations.** We use  
 169 archival photometry from the Hubble UV Globular Clus-  
 170 ter Survey (HUGS) (Piotto et al. 2015; Milone et al.  
 171 2017) in the F275W and F814W passbands to charac-  
 172 terize multiple populations in NGC 2808 (Milone et al.  
 173 2015a,b) (This data is available on MAST, Piotto 2018).  
 174 Additionally, we present a likelihood analysis of the pho-  
 175 tometric data of NGC 2808 to determine the number of  
 176 populations present in the cluster.

## 177 2. CHEMICAL CONSISTENCY

178 There are three primary areas in which must the stel-  
 179 lar models must be made chemically consistent: the at-  
 180 mospheric boundary conditions, the opacities, and inte-  
 181 rior abundances. The interior abundances are relatively  
 182 easily handled by adjusting parameters within our stel-  
 183 lar evolutionary code. However, the other two areas  
 184 are more complicated to bring into consistency. Atmo-  
 185 spheric boundary conditions and opacities must both  
 186 be calculated with a consistent set of chemical abun-  
 187 dances outside of the stellar evolution code. **Nearly all**  
 188 **prior efforts at modeling multiple stellar popula-**  
 189 **tions in globular clusters have adjusted the abun-**  
 190 **dances used in the atmospheric interior models,**  
 191 **and in the high temperature opacities, but have**  
 192 **not self-consistently modified the corresponding**  
 193 **low-temperature opacities and surface boundary**  
 194 **conditions, as these are found from stellar atmo-**  
 195 **sphere codes, and not the stellar interior codes**  
 196 **which are used to create stellar models and**  
 197 **isochrones. In this work, as in Dotter (2016),**  
 198 **the stellar interior models are chemically self-**  
 199 **consistent with the stellar atmosphere models.**  
 200 For evolution we use The Dartmouth Stellar Evolution Pro-  
 201 gram (DSEP) (Dotter et al. 2008), a well tested 1D  
 202 stellar evolution code which has a particular focus on  
 203 modelling low mass stars ( $\leq 2 M_{\odot}$ )

### 204 2.1. Atmospheric Boundary Conditions

205 Certain assumptions, primarily that the radiation field  
 206 is at equilibrium and radiative transport is diffusive

207 (Salaris & Cassisi 2005), made in stellar structure codes,  
 208 such as DSEP, are valid when the optical depth of a star  
 209 is large. However, in the atmospheres of stars, the num-  
 210 ber density of particles drops low enough and the opti-  
 211 cal depth consequently becomes small enough that these  
 212 assumptions break down, and separate, more physically  
 213 motivated, plasma modeling code is required. Generally  
 214 structure code will use tabulated atmospheric boundary  
 215 conditions generated by these specialized codes, such  
 216 as ATLAS9 (Kurucz 1993), PHOENIX (Husser et al.  
 217 2013), MARCS (Gustafsson et al. 2008), and MPS-  
 218 ATLAS (Kostogryz et al. 2023). Often, as the boundary  
 219 conditions are expensive to compute, they are not up-  
 220 dated as interior abundances vary.

221 One key element when chemically consistently mod-  
 222 eling NGC 2808 modeling is the incorporation of new  
 223 atmospheric models with the same elemental abun-  
 224 dances as the structure code. We use atmospheres  
 225 generated from the MARCS grid of model atmospheres  
 226 (Plez 2008). MARCS provides one-dimensional, hydro-  
 227 static, plane-parallel and spherical LTE atmospheric  
 228 models (Gustafsson et al. 2008). Model atmospheres  
 229 are made to match the spectroscopically measured ele-  
 230 mental abundances of Milone et al. (2015a) populations  
 231 A and E. Moreover, for each population, atmospheres  
 232 with various helium mass fractions are generated. These  
 233 range from  $Y=0.24$  to  $Y=0.36$  in steps of 0.03. All at-  
 234 mospheric models are computed to an optical depth of  
 235  $\tau = 100$  where their temperature and pressures serves as  
 236 boundary conditions for the structure code. In general,  
 237 enhancing helium in the atmosphere has only a small  
 238 impact on the atmospheric temperature profile, while  
 239 leading to a drop in the pressure by  $\sim 10 - 20\%$ .

### 240 2.2. Opacities

241 In addition to the atmospheric boundary conditions,  
 242 both the high and low temperature opacities used by  
 243 DSEP must be made chemically consistent. Here we  
 244 use OPLIB high temperature opacity tables (Colgan  
 245 et al. 2016) retrieved using the TOPS web-interface.  
 246 Retrieval of High temperature opacities is done us-  
 247 ing pyTOPSScrape, first introduced in Boudreaux &  
 248 Chaboyer (2023). Low temperature opacity tables are  
 249 retrieved from the Aesopus 2.0 web-interface (Marigo &  
 250 Aringer 2009; Marigo et al. 2022). Ideally, these opaci-  
 251 ties would be the same used in the atmospheric models.  
 252 However, the opacities used in the MARCS models are  
 253 not publicly available. As such, we use the opacities pro-  
 254 vided by the TOPS and Aesopus 2.0 web-interfaces.

## 255 3. STELLAR MODELS

256 We use the Dartmouth Stellar Evolution Program  
 257 (DSEP, Dotter et al. 2008) to generate stellar models.

**Table 1.** Population Composition

258 DSEP is a one-dimensional stellar evolution code which  
 259 includes a mixing length model of convection, gravi-  
 260 tational settling, and diffusion. Using the solar com-  
 261 position presented in (Grevesse et al. 2007) (GAS07),  
 262 MARCS model atmospheres, OPLIB high temperature  
 263 opacities, and AESOPUS 2.0 low temperature opaci-  
 264 ties we find a solar calibrated mixing length parameter,  
 265  $\alpha_{MLT}$ , of  $\alpha_{MLT} = 1.901$ . **Abundance measurements**  
 266 **are derived from Population A and E in Milone**  
 267 **et al. (2015a) (for P1 and P2 respectivley).**  
 268 We use DSEP to evolve stellar models ranging in mass  
 269 from 0.3 to 2.0 solar masses from the fully convective  
 270 pre-main sequence to the tip of the red giant branch.  
 271 Below  $0.7 M_{\odot}$  we evolve a model every  $0.03 M_{\odot}$  and  
 272 above  $0.7 M_{\odot}$  we evolve a model every  $0.05 M_{\odot}$ . We  
 273 evolve models over a grid of mixing length parameters  
 274 from  $\alpha_{MLT} = 1.0$  to  $\alpha_{MLT} = 2.0$  in steps of 0.1. For  
 275 each mixing length, a grid of models and isochrones were  
 276 calculated, with chemical compositions consistent with  
 277 Milone et al. (2015a) Populations A and E (see Tables  
 278 1 and 1) and a range of helium abundances ( $Y=0.24$ ,  
 279  $0.27$ ,  $0.30$ ,  $0.33$ ,  $0.36$ , and  $0.39$ ). In total, 144 sets of  
 280 isochrones, each with a unique composition and mixing  
 281 length were calculated. Each model is evolved in DSEP  
 282 with typical numeric tolerances of one part in  $10^7$ . Each  
 283 model is allowed a maximum time step of 50 Myr.

284 For each combination of population,  $Y$ , and  $\alpha_{MLT}$   
 285 we use the isochrone generation code first presented in  
 286 Dotter (2016) to generate a grid of isochrones. The  
 287 isochrone generation code identified equivalent evolu-  
 288 tionary points (EEPs) over a series of masses and inter-  
 289 polates between them. The grid of isochrones generated  
 290 for this work is available as a digital supplement to this  
 291 paper [10.5281/zenodo.10631439](https://doi.org/10.5281/zenodo.10631439). Given the complexity  
 292 of the parameter space when fitting multiple populations  
 293 along with the recent warnings in the literature regard-  
 294 ing overfitting datasets (e.g. Valle et al. 2022) we want  
 295 to develop a more objective way of fitting isochrones to  
 296 photometry than if we were to mark median ridge line  
 297 positions by hand.

298 **4. FIDANKA**

299 When fitting isochrones to the clusters with multiple  
 300 populations we have four main criteria for any method

| Element | Pop A (P1) | Pop E (P2) | Element | Pop A (P1) | Pop E (P2) |
|---------|------------|------------|---------|------------|------------|
| Li      | -0.08      | —          | In      | -1.46      | —          |
| Be      | 0.25       | —          | Sn      | -0.22      | —          |
| B       | 1.57       | —          | Sb      | -1.25      | —          |
| C       | 6.87       | 5.91       | Te      | -0.08      | —          |
| N       | 6.42       | 6.69       | I       | -0.71      | —          |
| O       | 7.87       | 6.91       | Xe      | -0.02      | —          |
| F       | 3.43       | —          | Cs      | -1.18      | —          |
| Ne      | 7.12       | 6.7        | Ba      | 1.05       | —          |
| Na      | 5.11       | 5.7        | La      | -0.03      | —          |
| Mg      | 6.86       | 6.42       | Ce      | 0.45       | —          |
| Al      | 5.21       | 6.61       | Pr      | -1.54      | —          |
| Si      | 6.65       | 6.77       | Nd      | 0.29       | —          |
| P       | 4.28       | —          | Pm      | -99.0      | —          |
| S       | 6.31       | 5.89       | Sm      | -1.3       | —          |
| Cl      | -1.13      | 4.37       | Eu      | -0.61      | —          |
| Ar      | 5.59       | 5.17       | Gd      | -1.19      | —          |
| K       | 3.9        | —          | Tb      | -1.96      | —          |
| Ca      | 5.21       | —          | Dy      | -1.16      | —          |
| Sc      | 2.02       | —          | Ho      | -1.78      | —          |
| Ti      | 3.82       | —          | Er      | -1.34      | —          |
| V       | 2.8        | —          | Tm      | -2.16      | —          |
| Cr      | 4.51       | —          | Yb      | -1.42      | —          |
| Mn      | 4.3        | —          | Lu      | -2.16      | —          |
| Fe      | 6.37       | —          | Hf      | -1.41      | —          |
| Co      | 3.86       | —          | Ta      | -2.38      | —          |
| Ni      | 5.09       | —          | W       | -1.41      | —          |
| Cu      | 3.06       | —          | Re      | -2.0       | —          |
| Zn      | 2.3        | —          | Os      | -0.86      | —          |
| Ga      | 0.78       | —          | Ir      | -0.88      | —          |
| Ge      | 1.39       | —          | Pt      | -0.64      | —          |
| As      | 0.04       | —          | Au      | -1.34      | —          |
| Se      | 1.08       | —          | Hg      | -1.09      | —          |
| Br      | 0.28       | —          | Tl      | -1.36      | —          |
| Kr      | 0.99       | —          | Pb      | -0.51      | —          |
| Rb      | 0.26       | —          | Bi      | -1.61      | —          |
| Sr      | 0.61       | —          | Po      | -99.0      | —          |
| Y       | 1.08       | —          | At      | -99.0      | —          |
| Zr      | 1.45       | —          | Rn      | -99.0      | —          |
| Nb      | -0.8       | —          | Fr      | -99.0      | —          |
| Mo      | -0.38      | —          | Ra      | -99.0      | —          |
| Tc      | -99.0      | —          | Ac      | -99.0      | —          |
| Ru      | -0.51      | —          | Th      | -2.2       | —          |
| Rh      | -1.35      | —          | Pa      | -99.0      | —          |
| Pd      | -0.69      | —          | U       | -2.8       | —          |

301 • The method must be robust enough to work along  
 302 the entire main sequence, turn off, and much of  
 303 the subgiant and red giant branch.

NOTE—Relative Metal composition used where  $a(\text{H}) = 12$ . Where the relative  
 composition is the the same for both Milone et al. (2015a) populations A and  
 E it is only listed in the population A column for the sake of visual clarity.

References—Milone et al. (2015a)

**Table 2.** Population Abundance Ratios

| Population | [Fe/H] | [ $\alpha$ /Fe] | [C/Fe] | [N/Fe] | [O/Fe] | [r/Fe] | [s/Fe] | C/O  | X      | Y      | Z       |
|------------|--------|-----------------|--------|--------|--------|--------|--------|------|--------|--------|---------|
| A(1)       | -1.13  | 0.32            | -0.43  | -0.28  | 0.31   | -1.13  | -1.13  | 0.10 | 0.7285 | 0.2700 | 0.00154 |
| E(2)       | -1.13  | -0.11           | -1.39  | -0.02  | -0.66  | -1.13  | -1.13  | 0.10 | 0.7594 | 0.240  | 0.00063 |

NOTE—Abundance Ratios for populations Milone et al. (2015a) A and E in NGC 2808.

**References**—Milone et al. (2015a)

- Any method should consider photometric uncertainty in the fitting process.
- The method should be model independent, weighting any n number of populations equally.
- The method should be automated and require minimal intervention from the user.

We do not believe that any currently available software is a match for our use case. Therefore, we elect to develop our own software suite, *Fidanka*. *Fidanka* is a python package designed to automate much of the process of measuring fiducial lines in CMDs, adhering to the four criteria we lay out above. Primary features of *Fidanka* may be separated into three categories: fiducial line measurement, stellar population synthesis, and isochrone optimization/fitting. Additionally, there are utility functions that are detailed in the *Fidanka* documentation.

#### 4.1. Fiducial Line Measurement

*Fidanka* takes an iterative approach to measuring fiducial lines, the first step of which is to make a “guess” as to the fiducial line. This initial guess is calculated by splitting the CMD into magnitude bins, with uniform numbers of stars per bin (so that bins cover a small magnitude range over densely populated regions of the CMD while covering a much larger magnitude range in sparsely populated regions of the CMD, such as the RGB). A unimodal Gaussian distribution is then fit to the color distribution of each bin, and the resulting mean color is used as the initial fiducial line guess. This rough fiducial line will approximately trace the area of highest density. The initial guess will be used to verticalize the CMD so that further algorithms can work in 1-D magnitude bins without worrying about weighting issues caused by varying projections of the evolutionary sequence onto the magnitude axis. Verticalization is performed taking the difference between the guess fiducial line and the color of each star in the CMD.

If *Fidanka* were to simply apply the same algorithm to the verticalized CMD then the resulting fiducial line

would likely be a re-extraction of the initial fiducial line guess. To avoid this, we take a more robust, number density based approach, which considers the distribution of stars in both color and magnitude space simultaneously. **As an example, in the case of this work,** for each star in the CMD we first use an `introslect` partitioning algorithm to select the 50 nearest stars in F814W vs. F275W-F814W space. **It should be noted that unlike methods using chromosome maps Fidanka only considers two filters and therefore may lose access to information better traced by other filters.** To account for the case where the star is at an extreme edge of the CMD, those 50 stars include the star itself (such that we really select 49 stars + 1). We use `qhull`<sup>1</sup>(Barber et al. 1996) to calculate the convex hull of those 50 points. The number density at each star then is defined as  $50/A_{hull}$ , where  $A_{hull}$  is the area of the convex hull. Because we use a fixed number of points per star, and a partitioning algorithm as opposed to a sorting algorithm, this method scales like  $\mathcal{O}(n)$ , where  $n$  is the number of stars in the CMD. This method also intrinsically weights the density of each star equally as the counting statistics per bin are uniform. We are left with a CMD where each star has a defined number density (Figure 1).

*Fidanka* can now exploit this density map to fit a better fiducial line to the data, as the density map is far more robust to outliers. There are multiple algorithms we implement to fit the fiducial line to the color-density profile in each magnitude bin (Figure 2); they are explained in more detail in the *Fidanka* documentation. However, of most relevance here is the Bayesian Gaussian Mixture Modeling (BGMM) method. BGMM is a clustering algorithm which, for some fixed number of  $n$ -dimensional Gaussian distributions,  $K$ , determines the mean, covariance, and mixing probability (somewhat analogous to amplitude) of each  $k^{th}$  distribution, such

<sup>1</sup> <https://www.qhull.com>

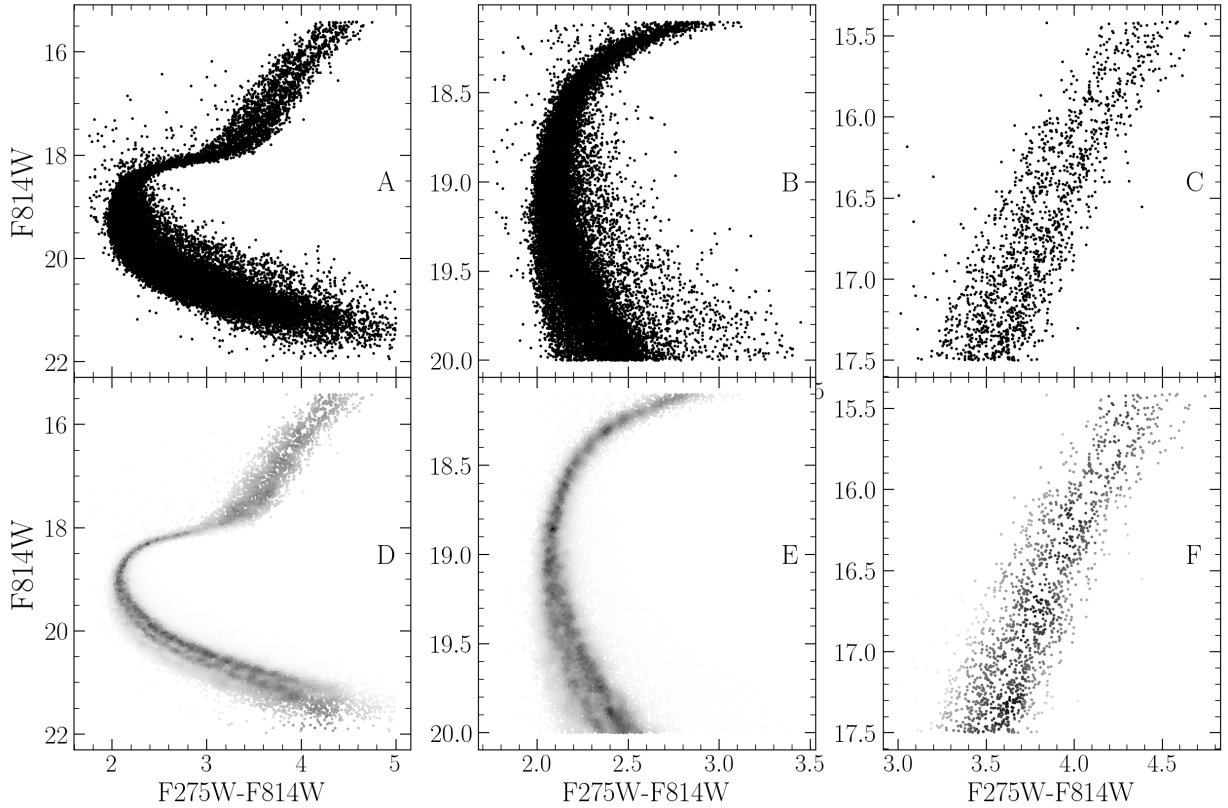


**Figure 1.** Figures in the top row are the raw CMD, while figures in the bottom row are colored by the density map. Density map demo showing density estimate over different parts of the evolutionary sequence. The left panel shows the density map over the entire evolutionary sequence, while the middle panel shows the density map over the main sequence and the right most panel shows the density map over the RGB.

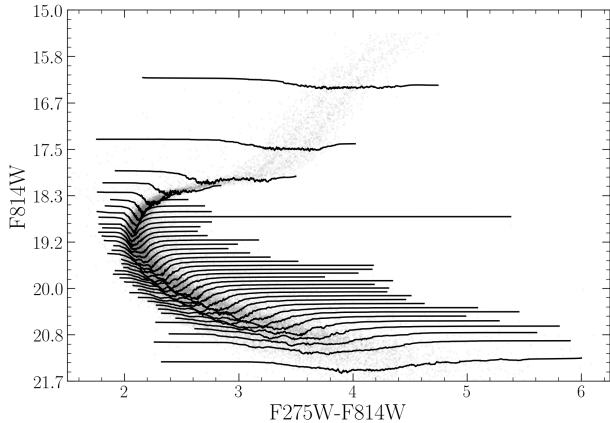


**Figure 2.** CMD where point brightness is determined by local density. Lines show the density-color profile in each magnitude bin. In this figure adaptive binning targeted 1000 stars per bin

380 that the local lower bound of the likelihood of each star  
 381 belonging strongly to a single distribution is maximized.  
 382 Maximization is performed using the Dirichlet process,  
 383 which is a non-parametric Bayesian method of  
 384 determining the number of Gaussian distributions,  $K$ ,

385 which best fit the data (Ferguson 1973; Pedregosa et al.  
 386 2011). Use of the Dirichlet process allows for dynamic  
 387 variation in the number of inferred populations from  
 388 magnitude bin to magnitude bin. Specifically, popula-  
 389 tions are clearly visually separated from the lower main  
 390 sequence through the turn off; however, at the turn off  
 391 and throughout much of the subgiant branch, the two  
 392 visible populations overlap due to their extremely simi-  
 393 lar ages (i.e. Jordán et al. 2002). The Dirichlet process  
 394 allows for the BGMM method to infer a single popula-  
 395 tion in these regions, while inferring two populations in  
 396 regions where they are clearly separated. More gener-  
 397 ally, the use of the Dirichlet process removes the need  
 398 for a prior on the exact number of populations to fit.  
 399 Rather, the user specifies a upper bound on the num-  
 400 ber of populations within the cluster. An example bin  
 401 ( $F814W = 20.6$ ) is shown in Figure 3.

402 Fidanka's BGMM method first breaks down the verti-  
 403 calized CMD into magnitude bins with uniform num-  
 404 bers of stars per bin (here we adopt 250). Any stars  
 405 left over are placed into the final bin. For each bin a  
 406 BGMM model with a maximum of 5 populations is fit  
 407 to the color density profile. The number of populations

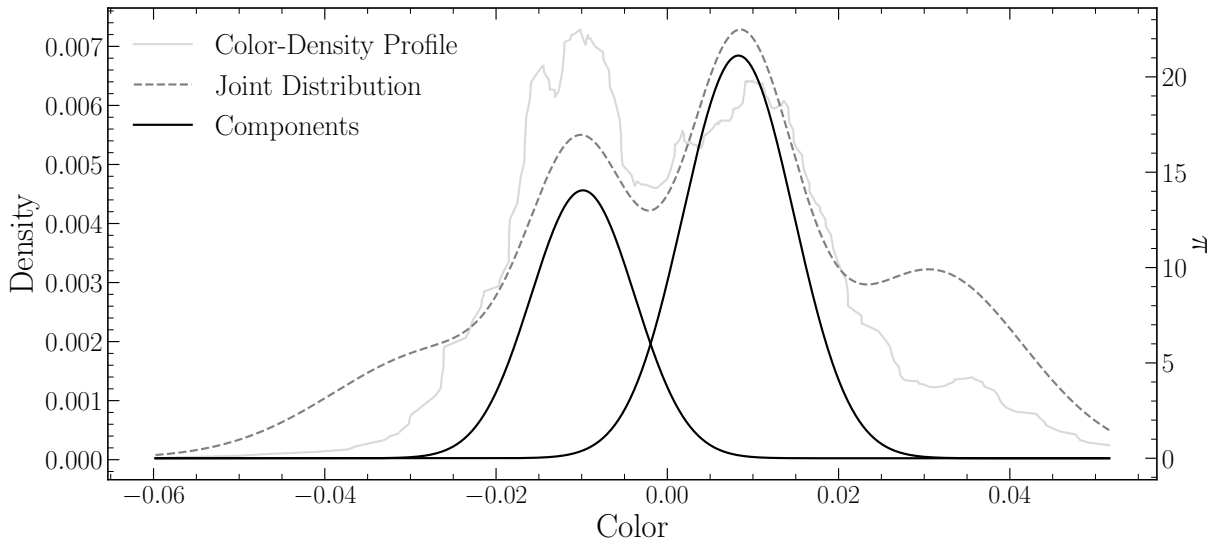


**Figure 3.** Example of BGMM fit to a magnitude bin. The grey line shows the underlying color-density profile, while the black dashed-line shows the joint distribution of each BGMM component. The solid black lines show the two selected components.

is then inferred from the weighting parameter (the mixing probability) of each population. If the weighting parameter of any  $k^{th}$  components less than 0.05, then that component is considered to be spurious and removed. Additionally, if the number of populations in the bin above and the bin below are the same, then the number of populations in the current bin is forced to be the same as the number of populations in the bin above. Finally, the initial guess fiducial line is added back to the BGMM inferred line. Figure 4 shows the resulting fiducial line(s) in each magnitude bin for both a verticalized CMD and a non verticalized CMD. In contrast to other work in the literature where evidence for up to 5 distinct populations has been found; we only find evidence for two stellar populations.

This method of fiducial line extraction effectively discriminated between multiple populations along the main sequence and RGB of a cluster, while simultaneously allowing for the presence of a single population along the MSTO and subgiant branch.

We can adapt this density map based BGMM method to consider photometric uncertainties by adopting a simple Monte Carlo approach. Instead of measuring the fiducial line(s) a single time, *Fidanka* can measure the fiducial line(s) many times, resampling the data with replacement each time. For each resampling *Fidanka* adds a random offset to each filter based on the photometric uncertainties of each star. From these  $n$  measurements the mean fiducial line for each sequence can be identified along with upper and lower bound confidence intervals in each magnitude bin.

#### 4.2. Stellar Population Synthesis

While not extensively used in this paper *Fidanka* can, in addition to measuring fiducial lines, perform stellar population synthesis. *Fidanka*'s population synthesis module can generate synthetic stellar population from a set of MIST formatted isochrones. This is of primary importance for binary population modeling. The module is also used to generate synthetic CMDs for the purpose of testing the fiducial line extraction algorithms against priors.

*Fidanka* uses MIST formatted isochrones (Dotter 2016) as input along with distance modulus, B-V color excess, binary mass fraction, and bolometric corrections. An arbitrarily large number of isochrones may be used to define an arbitrary number of populations. Synthetic stars are samples from each isochrone based on a definable probability (for example it is believed that  $\sim 90\%$  of stars in globular clusters are younger population (e.g. Suntzeff & Kraft 1996; Carretta 2013)). Based on the metallicity,  $\mu$ , and E(B-V) of each isochrone, bolometric corrections are taken from bolometric correction tables. Where bolometric correction tables do not include exact metallicities or extinctions a linear interpolation is performed between the two bounding values.

#### 4.3. Isochrone Optimization

The optimization routines in *Fidanka* will find the best fit distance modulus, B-V color excess, and binary number fraction for a given set of isochrones. If a single isochrone is provided then the optimization is done by minimizing the  $\chi^2$  of the perpendicular distances between an isochrone and a fiducial line. If multiple isochrones are provided then those isochrones are first used to run stellar population synthesis and generate a

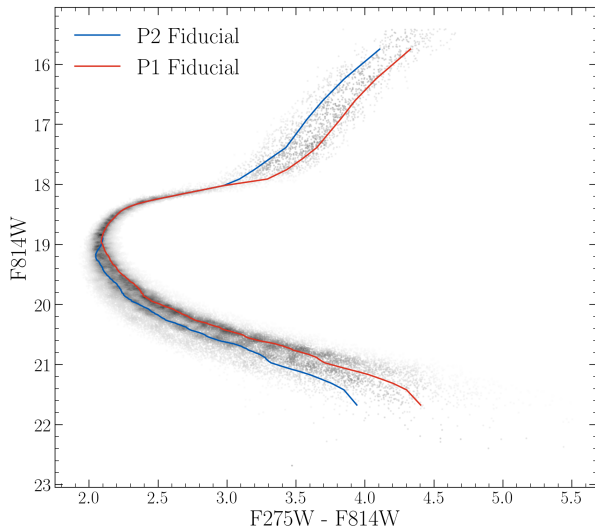
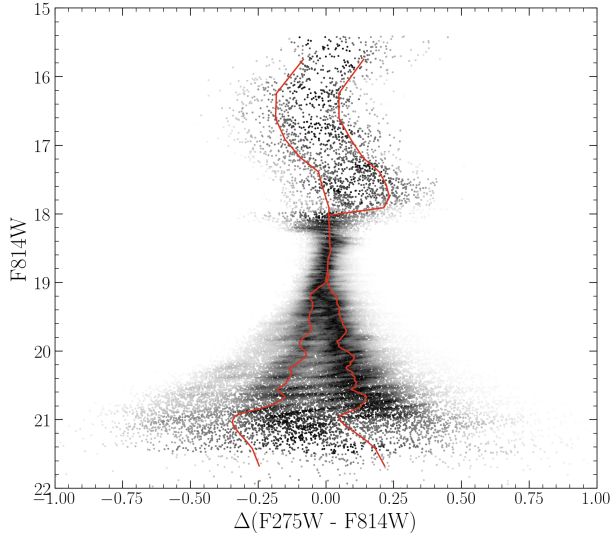


**Figure 4.** Verticalized CMD (where the color of each data point is subtracted from the color of the fiducial line at that magnitude) where point brightness is determined by density (top). CMD where point brightness is determined by density, calculated fiducial lines are shown (bottom). The data used is from the Hubble Space Telescope UV Legacy Survey of Galactic Globular Clusters.

472 synthetic CMD. The optimization is then done by min-  
 473 imizing the  $\chi^2$  of both the perpendicular distances be-  
 474 tween and widths of the observed fiducial line and the  
 475 fiducial line of the synthetic CMD.

#### 4.4. *Fidanka* Testing

476  
 477 In order to validate *fidanka* we have run an series of  
 478 injection recovery tests using *Fidanka*'s population syn-  
 479 thesis routines to build various synthetic populations  
 480 and *Fidanka*'s fiducial measurement routines to recover  
 481 these populations. Each population was generated us-

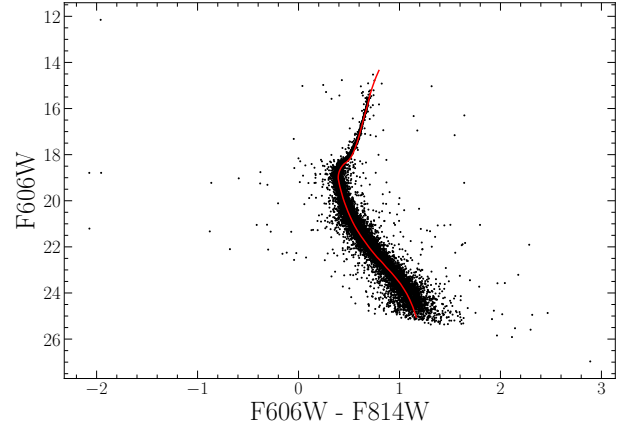


**Figure 5.** Synthetic population generated by *fidanka* at 10000pc with  $E(B-V) = 0$ , and an age of 12 Gyr along with the best fitting isochrone. The best fit parameters are derived to be  $\mu = 15.13$ ,  $E(B-V)=0.001$ , and an age of 12.33 Gyr.

482 ing the initial mass function given in (Milone et al. 2012)  
 483 for the redmost population ( $\alpha = -1.2$ ). Further, every  
 484 population was given a binary population fraction of  
 485 10%, distance uniformly sampled between 5000pc and  
 486 15000pc, and a B-V color excess uniformly sampled be-  
 487 tween 0 and 0.1. *Fidanka* makes uses of ACS arti-  
 488 ficial star tests (Anderson et al. 2008) to model  
 489 the noise and completeness of a synthetic popu-  
 490 lation in passbands covered by those tests. Full  
 491 details on how *Fidanka* uses artificial star tests  
 492 may be found on its documentation page<sup>2</sup> Finally,  
 493 each synthetic population was generated using a fixed  
 494 age uniformly sampled between 7 Gyr and 14 Gyr. An  
 495 example synthetic population along with its associated  
 496 best fit isochrone are shown in Figure 5.

497 For each trial we use *Fidanka* to measure the fiducial  
 498 line and then optimize that fiducial line against the orig-  
 499 inating isochrone to estimate distance modulus, age, and  
 500 color B-V excess. Figure 6 is built from 1000 Monte-  
 501 Carlo trials and shows the mean and width of the per-  
 502 cent error distributions for  $\mu$ ,  $A_v$ , and age. In general  
 503 *Fidanka* is able to recover distance moduli effectively  
 504 with age and  $E(B-V)$  recovery falling in line with other  
 505 literature that does not consider the CMD outside of the  
 506 main sequence, main sequence turn off, sub giant, and  
 507 red giant branches; specifically, it should be noted that  
 508 *Fidanka* is not setup to model the horizontal branch.

## 5. ISOCHRONE FITTING

509  
 510 We fit pairs of isochrones to the HUGS data for NGC  
 511 2808 using *Fidanka*, as described in §4. As was men-

<sup>2</sup> <https://tboudreaux.github.io/fidanka/>

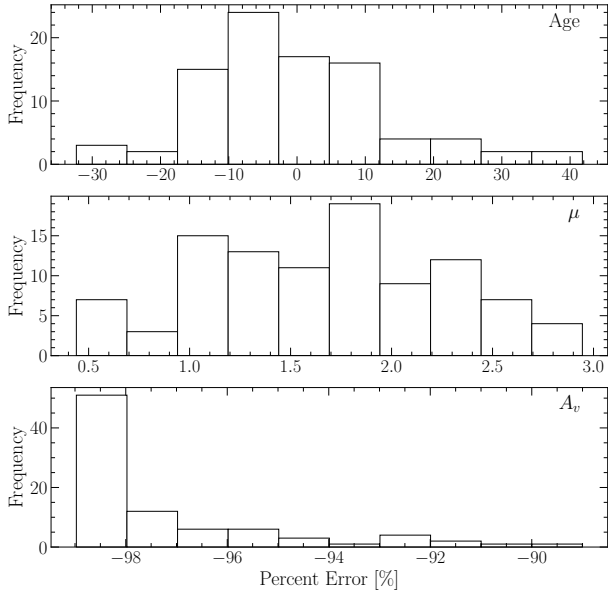


**Figure 6.** Percent Error distribution for each of the three deriver parameters. Note that these values will be sensitive to the magnitude uncertainties of the photometry. Here we made use of the ACS artificial star tests to estimate the uncertainties.

tioned in §4.1 the method used by Fidanka only considers two filters — in the case of this work F275W and F814W — and therefore may be unable to distinguish between populations separated only in the higher-dimensional space of a chromosome map. For further discussion of why we adopt this method, despite its limits, we refer the reader to §5.1. Two isochrones, one for P1 and one for P2 are fit simultaneously. These isochrones are constrained to have distance modulus,  $\mu$ , and color excess,  $E(B-V)$  which agree to within 0.5% and an ages which agree to within 1%. Moreover, we constrain the mixing length,  $\alpha_{ML}$ , for any two isochrones in a set to be within 0.5 of one and other. For every isochrone in the set of combination of which fulfilling these constraints  $\mu$ ,  $E(B-V)$ ,  $Age_A$ , and  $Age_B$  are optimized to reduce the  $\chi^2$  distance ( $\chi^2 = \sum \sqrt{\Delta color^2 + \Delta mag^2}$ ) between the fiducial lines and the isochrones. Because we fit fiducial lines directly, we do not need to consider the binary population fraction,  $f_{bin}$ , as a free parameter.

The best fit isochrones are shown in Figure 7 and optimized parameters for these are presented in Table 1. The initial guess for the age of these populations was locked to 12 Gyr and the initial Extinction was locked to 0.5 mag. The initial guess for the distance modulus was determined at run time using a dynamic time warping algorithm to best align the morphologies of the fiducial line

with the target isochrone. This algorithm is explained in more detail in the Fidanka documentation under the function called `guess_mu`. We find helium mass fractions that are consistent with those identified in past literature (e.g. Milone et al. 2015a). Note that our helium mass fraction grid has a spacing of 0.03 between grid points and we are therefore unable to resolve between certain proposed helium mass fractions for the younger sequence (for example between 0.37 and 0.39). We also note that the best fit mixing length parameter which we derive for P1 and P2 do not agree within their uncertainties. This is not surprising as the much higher mean molecular mass of P2 — when compared to P1, due to population P2’s larger helium mass fraction — will result in a steeper adiabatic temperature gradient

Past literature (e.g. Milone et al. 2015a, 2018) have found helium mass fraction variation from the redmost to bluemost populations of  $\sim 0.12$ . Here we find a helium mass fraction variation of 0.15 which, given the spacing of the helium grid we use is consistent with these past results. The helium mass fractions we derive for P1 and P2 are consistent with those of populations A and E in Milone et al. (2015a); however, populations B+C and D in that study are more prominently separated in the F275W-F814W colorband. The inferred helium mass fractions for P1 and P2 are not consistent, with those reported for populations B+C and D.

### 5.1. The Number of Populations in NGC 2808

In order to estimate the number of populations which ideally fit the NGC 2808 F275W-F814W photometry without overfitting the data we make use of silhouette analysis (Rousseeuw 1987, and in a similar manner to how Valle et al. (2022) perform their analysis of spectroscopic data). We find the average silhouette score for all tagged clusters identified using BGMM in all magnitude bins over the CMD using the standard python module `sklearn`. Figure 8 shows the silhouette analysis results and that two populations fit the photometry most ideally. This is in line with what our BGMM model predicts for the majority of the the CMD.

While we make use a purely CMD based approach in this work, other literature has made use of Chromosome Maps. These consist of implicitly verticalized pseudo colors. In the chromosome map for NGC 2808 there may be evidence for more than two populations; further, the chromosome maps used include information from additional filters (F336W and

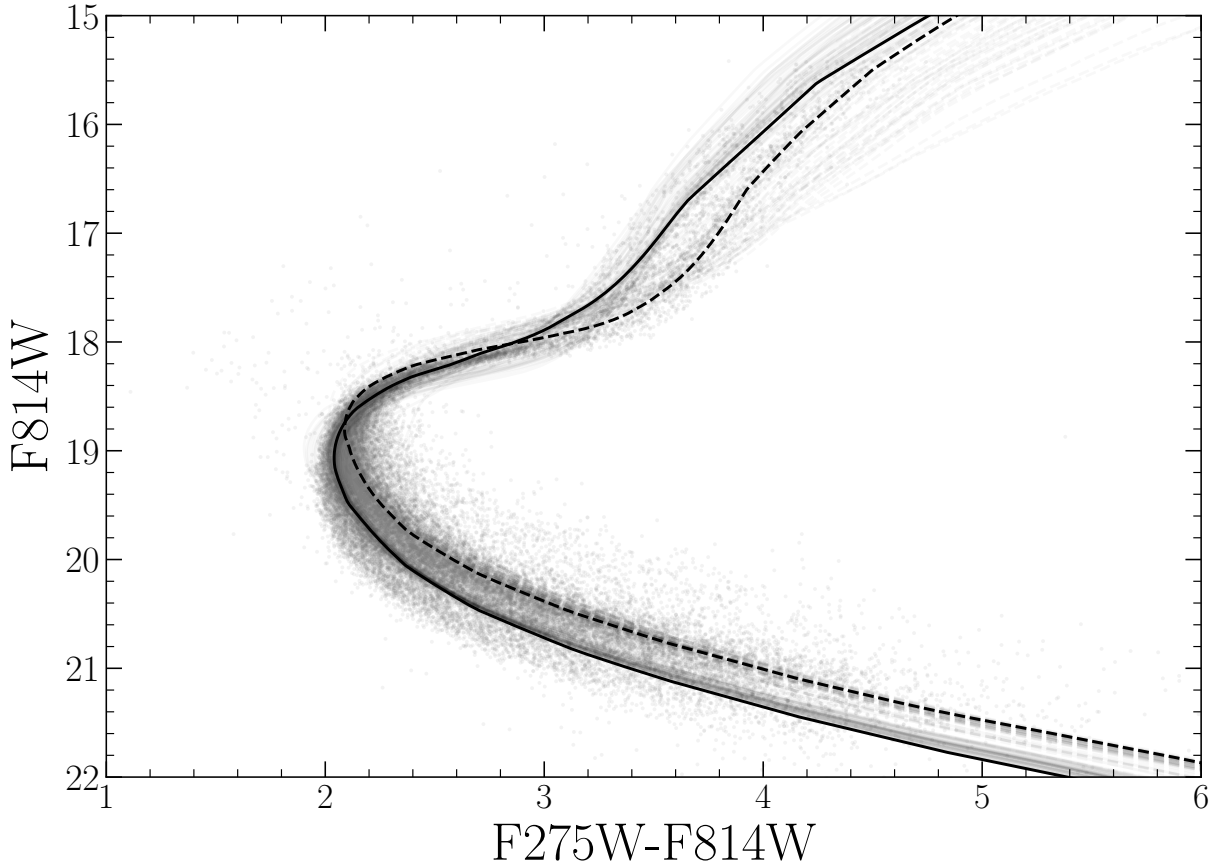


**Figure 7.** Best fit isochrone results for NGC 2808. The best fit P1 and P2 models are shown as black lines. The following 50 best fit models are presented as grey lines. The dashed black line is fit to P1, while the solid black line is fit to P2.

| Population | Age<br>[Gyr]             | Distance Modulus | Extinction<br>[mag] | Y    | $\alpha_{ML}$ | $\chi^2_\nu$ |
|------------|--------------------------|------------------|---------------------|------|---------------|--------------|
| P1         | $12.996^{+0.87}_{-0.64}$ | 15.021           | 0.54                | 0.24 | 2.050         | 0.021        |
| P2         | $13.061^{+0.86}_{-0.69}$ | 15.007           | 0.537               | 0.39 | 1.600         | 0.033        |

**Table 1.** Best fit parameters derived from fitting isochrones to the fiducial lines derived from the NCG 2808 photometry. The one sigma uncertainty reported on population age were determined from the 16th and 84th percentiles of the distribution of best fit isochrones ages.

591 F438W) which we do not use in our CMD ap-  
 592 proach. The process of transforming magni-  
 593 tude measurements into chromosome space re-  
 594 sults in dramatically increased uncertainties for  
 595 each star. We find a mean fractional uncertainty  
 596 for chromosome parameters —  $\Delta_{F275W,F814W}$  and  
 597  $\Delta_{CF275W,F336W,F438W}$  — of  $\approx 1$  (Figure 9) when  
 598 starting with magnitude measurements having  
 599 a mean best-case (i.e. uncertainty assumed to  
 600 only be due to Poisson statistics) fractional un-  
 601 certainty of  $\approx 0.0005$ . Fractional uncertainties  
 602 for chromosome parameters were calculated via  
 603 standard propagation of uncertainty. Because of

604 how Fidanka operates, i.e. resampling a proba-  
 605 bility distribution for each star in order to iden-  
 606 tify clusters, we are unable to make statisti-  
 607 cally meaningful statements from the chromo-  
 608 some map

## 609 6. CONCLUSION

610 Here we have performed the first chemically self-  
 611 consistent modeling of the Milky Way Globular Cluster  
 612 NGC 2808. We find that, updated atmospheric bound-  
 613 ary conditions and opacity tables do not have a signif-  
 614 icant effect on the inferred helium abundances of mul-  
 615 tiple populations. Specifically, we find that population  
 616 has a helium mass fraction of 0.24, while population E

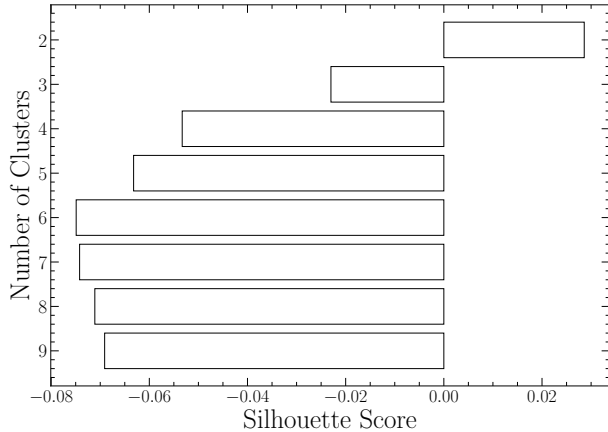


**Figure 8.** Silhouette analysis for NGC 2808 F275W-F814W photometry. The Silhouette scores are an average of score for each magnitude bin. Positive scores indicate that the clustering algorithm produced well distinguished clusters while negative scores indicate clusters which are not well distinguished.

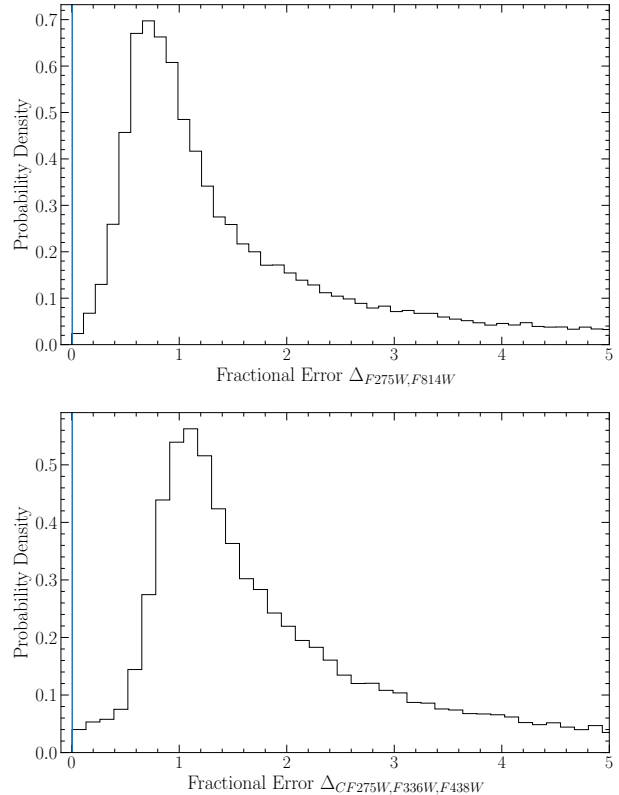


**Figure 9.** Fractional error distribution of  $\Delta_{F275W,F814W}$  (top) and  $\Delta_{CF275W,F336W,F438W}$ . The vertical line near 0 in each figure indicates the mean fractional error of the magnitude measurements used to find the chromosome parameters.

617 has a helium mass fraction of 0.39. Additionally, we  
 618 find that the ages of these two populations agree within  
 619 uncertainties. We only find evidence for two distinct  
 620 stellar populations, which is in agreement with recent  
 621 work studying the number of populations in NGC 2808  
 622 spectroscopic data.

623 We introduce a new software suite for globular cluster  
 624 science, **Fidanka**, which has been released under a per-  
 625 missive open source license. **Fidanka** aims to provide a  
 626 statistically robust set of tools for estimating the param-  
 627 eters of multiple populations within globular clusters.

628 This work has made use of the NASA astrophysical data  
 629 system (ADS). We would like to thank Elisabeth New-  
 630 ton and Aaron Dotter for their support and for useful  
 631 discussion related to the topic of this paper. Addition-  
 632 ally, we would like to thank Kara Fagerstrom, Aylin  
 633 Garcia Soto, and Keighley Rockcliffe for their useful  
 634 discussion related to in this work. We acknowledge the  
 635 support of a NASA grant (No. 80NSSC18K0634).

## REFERENCES

- 636 Alcaïno, G. 1975, *A&AS*, 21, 15
- 637 Anderson, J., Sarajedini, A., Bedin, L. R., et al. 2008, *AJ*,  
638 135, 2055, doi: [10.1088/0004-6256/135/6/2055](https://doi.org/10.1088/0004-6256/135/6/2055)
- 639 Barber, C. B., Dobkin, D. P., & Huhdanpaa, H. 1996, *ACM*  
640 *Transactions on Mathematical Software (TOMS)*, 22, 469
- 641 Bastian, N., & Lardo, C. 2015, *MNRAS*, 453, 357,  
642 doi: [10.1093/mnras/stv1661](https://doi.org/10.1093/mnras/stv1661)
- 643 Bastian, N., & Lardo, C. 2018, *Annual Review of*  
644 *Astronomy and Astrophysics*, 56, 83
- 645 Bekki, K., & Chiba, M. 2002, *The Astrophysical Journal*,  
646 566, 245, doi: [10.1086/337984](https://doi.org/10.1086/337984)
- 647 Boudreaux, E. M., & Chaboyer, B. C. 2023, *ApJ*, 944, 129,  
648 doi: [10.3847/1538-4357/acb685](https://doi.org/10.3847/1538-4357/acb685)
- 649 Boylan-Kolchin, M. 2018, *MNRAS*, 479, 1423,  
650 doi: [10.1093/mnras/sty1490](https://doi.org/10.1093/mnras/sty1490)
- 651 Brodie, J. P., & Strader, J. 2006, *Annu. Rev. Astron.*  
652 *Astrophys.*, 44, 193
- 653 Brown, J. H., Burkert, A., & Truran, J. W. 1991, *ApJ*, 376,  
654 115, doi: [10.1086/170260](https://doi.org/10.1086/170260)
- 655 —. 1995, *ApJ*, 440, 666, doi: [10.1086/175304](https://doi.org/10.1086/175304)
- 656 Cadelano, M., Dalessandro, E., Salaris, M., et al. 2022,  
657 *ApJL*, 924, L2, doi: [10.3847/2041-8213/ac424a](https://doi.org/10.3847/2041-8213/ac424a)
- 658 Carretta, E. 2006, *AJ*, 131, 1766, doi: [10.1086/499565](https://doi.org/10.1086/499565)
- 659 —. 2013, *A&A*, 557, A128,  
660 doi: [10.1051/0004-6361/201322103](https://doi.org/10.1051/0004-6361/201322103)
- 661 —. 2015, *ApJ*, 810, 148, doi: [10.1088/0004-637X/810/2/148](https://doi.org/10.1088/0004-637X/810/2/148)
- 662 Carretta, E., Bragaglia, A., & Cacciari, C. 2004, *ApJL*,  
663 610, L25, doi: [10.1086/423034](https://doi.org/10.1086/423034)
- 664 Carretta, E., Bragaglia, A., Gratton, R. G., et al. 2010,  
665 *Astronomy & Astrophysics*, 516, A55
- 666 Colgan, J., Kilcrease, D. P., Magee, N. H., et al. 2016, in  
667 *APS Meeting Abstracts*, Vol. 2016, APS Division of  
668 *Atomic, Molecular and Optical Physics Meeting*  
669 *Abstracts*, D1.008
- 670 de Mink, S. E., Pols, O. R., Langer, N., & Izzard, R. G.  
671 2009, *A&A*, 507, L1, doi: [10.1051/0004-6361/200913205](https://doi.org/10.1051/0004-6361/200913205)
- 672 Decressin, T., Meynet, G., Charbonnel, C., Prantzos, N., &  
673 Ekström, S. 2007, *A&A*, 464, 1029,  
674 doi: [10.1051/0004-6361:20066013](https://doi.org/10.1051/0004-6361:20066013)
- 675 Denissenkov, P. A., & Hartwick, F. D. A. 2014, *MNRAS*,  
676 437, L21, doi: [10.1093/mnras/slt133](https://doi.org/10.1093/mnras/slt133)
- 677 D’Ercole, A., D’Antona, F., Ventura, P., Vesperini, E., &  
678 McMillan, S. L. W. 2010, *MNRAS*, 407, 854,  
679 doi: [10.1111/j.1365-2966.2010.16996.x](https://doi.org/10.1111/j.1365-2966.2010.16996.x)
- 680 D’Ercole, A., Vesperini, E., D’Antona, F., McMillan, S.  
681 L. W., & Recchi, S. 2008, *MNRAS*, 391, 825,  
682 doi: [10.1111/j.1365-2966.2008.13915.x](https://doi.org/10.1111/j.1365-2966.2008.13915.x)
- 683 Dotter, A. 2016, *ApJS*, 222, 8,  
684 doi: [10.3847/0067-0049/222/1/8](https://doi.org/10.3847/0067-0049/222/1/8)
- 685 Dotter, A., Chaboyer, B., Jevremović, D., et al. 2008, *The*  
686 *Astrophysical Journal Supplement Series*, 178, 89
- 687 Dotter, A., Ferguson, J. W., Conroy, C., et al. 2015,  
688 *MNRAS*, 446, 1641, doi: [10.1093/mnras/stu2170](https://doi.org/10.1093/mnras/stu2170)
- 689 Ferguson, T. S. 1973, *The annals of statistics*, 209
- 690 Gratton, R., Sneden, C., & Carretta, E. 2004, *ARA&A*, 42,  
691 385, doi: [10.1146/annurev.astro.42.053102.133945](https://doi.org/10.1146/annurev.astro.42.053102.133945)
- 692 Gratton, R. G., Carretta, E., & Bragaglia, A. 2012,  
693 *Astronomy and Astrophysics Reviews*, 20, 50,  
694 doi: [10.1007/s00159-012-0050-3](https://doi.org/10.1007/s00159-012-0050-3)
- 695 Gratton, R. G., Lucatello, S., Carretta, E., et al. 2011,  
696 *A&A*, 534, A123, doi: [10.1051/0004-6361/201117690](https://doi.org/10.1051/0004-6361/201117690)
- 697 Grevesse, N., Asplund, M., & Sauval, A. J. 2007, *SSRv*,  
698 130, 105, doi: [10.1007/s11214-007-9173-7](https://doi.org/10.1007/s11214-007-9173-7)
- 699 Gustafsson, B., Edvardsson, B., Eriksson, K., et al. 2008,  
700 *A&A*, 486, 951, doi: [10.1051/0004-6361:200809724](https://doi.org/10.1051/0004-6361:200809724)
- 701 Hong, S., Lim, D., Chung, C., et al. 2021, *AJ*, 162, 130,  
702 doi: [10.3847/1538-3881/ac0ce6](https://doi.org/10.3847/1538-3881/ac0ce6)
- 703 Hudson, M. J., & Robison, B. 2018, *Monthly Notices of the*  
704 *Royal Astronomical Society*, 477, 3869,  
705 doi: [10.1093/mnras/sty844](https://doi.org/10.1093/mnras/sty844)
- 706 Husser, T. O., Wende-von Berg, S., Dreizler, S., et al. 2013,  
707 *A&A*, 553, A6, doi: [10.1051/0004-6361/201219058](https://doi.org/10.1051/0004-6361/201219058)
- 708 Jordán, A., Côté, P., West, M. J., & Marzke, R. O. 2002,  
709 *ApJL*, 576, L113, doi: [10.1086/343759](https://doi.org/10.1086/343759)
- 710 Kalirai, J. S., & Richer, H. B. 2010, *Philosophical*  
711 *Transactions of the Royal Society of London Series A*,  
712 368, 755, doi: [10.1098/rsta.2009.0257](https://doi.org/10.1098/rsta.2009.0257)
- 713 Kostogryz, N., Shapiro, A. I., Witzke, V., et al. 2023,  
714 *Research Notes of the AAS*, 7, 39,  
715 doi: [10.3847/2515-5172/acc180](https://doi.org/10.3847/2515-5172/acc180)
- 716 Kravtsov, A. V., & Gnedin, O. Y. 2005, *The Astrophysical*  
717 *Journal*, 623, 650
- 718 Kurucz, R.-L. 1993, *Kurucz CD-Rom*, 13
- 719 Lardo, C., Salaris, M., Cassisi, S., & Bastian, N. 2022,  
720 *A&A*, 662, A117, doi: [10.1051/0004-6361/202243843](https://doi.org/10.1051/0004-6361/202243843)
- 721 Latour, M., Husser, T. O., Giesers, B., et al. 2019, *A&A*,  
722 631, A14, doi: [10.1051/0004-6361/201936242](https://doi.org/10.1051/0004-6361/201936242)
- 723 Legnardi, M. V., Milone, A. P., Armillotta, L., et al. 2022,  
724 *MNRAS*, 513, 735, doi: [10.1093/mnras/stac734](https://doi.org/10.1093/mnras/stac734)
- 725 Marigo, P., & Aringer, B. 2009, *A&A*, 508, 1539,  
726 doi: [10.1051/0004-6361/200912598](https://doi.org/10.1051/0004-6361/200912598)
- 727 Marigo, P., Aringer, B., Girardi, L., & Bressan, A. 2022,  
728 *ApJ*, 940, 129, doi: [10.3847/1538-4357/ac9b40](https://doi.org/10.3847/1538-4357/ac9b40)
- 729 Marino, A. F., Milone, A. P., Karakas, A. I., et al. 2015,  
730 *Monthly Notices of the Royal Astronomical Society*, 450,  
731 815, doi: [10.1093/mnras/stv420](https://doi.org/10.1093/mnras/stv420)

- 732 Martocchia, S., Dalessandro, E., Lardo, C., et al. 2019,  
733 Monthly Notices of the Royal Astronomical Society, 487,  
734 5324, doi: [10.1093/mnras/stz1596](https://doi.org/10.1093/mnras/stz1596)
- 735 Milone, A. P., Piotto, G., Bedin, L. R., et al. 2012, ApJ,  
736 744, 58, doi: [10.1088/0004-637X/744/1/58](https://doi.org/10.1088/0004-637X/744/1/58)
- 737 Milone, A. P., Marino, A. F., Piotto, G., et al. 2015a, ApJ,  
738 808, 51, doi: [10.1088/0004-637X/808/1/51](https://doi.org/10.1088/0004-637X/808/1/51)
- 739 —. 2015b, MNRAS, 447, 927, doi: [10.1093/mnras/stu2446](https://doi.org/10.1093/mnras/stu2446)
- 740 Milone, A. P., Piotto, G., Renzini, A., et al. 2017, MNRAS,  
741 464, 3636, doi: [10.1093/mnras/stw2531](https://doi.org/10.1093/mnras/stw2531)
- 742 Milone, A. P., Marino, A. F., Renzini, A., et al. 2018,  
743 MNRAS, 481, 5098, doi: [10.1093/mnras/sty2573](https://doi.org/10.1093/mnras/sty2573)
- 744 Pasquato, M., & Milone, A. 2019, arXiv e-prints,  
745 arXiv:1906.04983, doi: [10.48550/arXiv.1906.04983](https://doi.org/10.48550/arXiv.1906.04983)
- 746 Pedregosa, F., Varoquaux, G., Gramfort, A., et al. 2011,  
747 Journal of Machine Learning Research, 12, 2825
- 748 Peebles, P. J. E., & Dicke, R. H. 1968, ApJ, 154, 891,  
749 doi: [10.1086/149811](https://doi.org/10.1086/149811)
- 750 Peng, E. W., Ferguson, H. C., Goudfrooij, P., et al. 2011,  
751 The Astrophysical Journal, 730, 23
- 752 Piotto, G. 2018, HST UV Globular Cluster Survey  
753 (“HUGS”), STScI/MAST, doi: [10.17909/T9810F](https://doi.org/10.17909/T9810F)
- 754 Piotto, G., Bedin, L. R., Anderson, J., et al. 2007, The  
755 Astrophysical Journal Letters, 661, L53,  
756 doi: [10.1086/518503](https://doi.org/10.1086/518503)
- 757 Piotto, G., Milone, A. P., Bedin, L. R., et al. 2015, AJ, 149,  
758 91, doi: [10.1088/0004-6256/149/3/91](https://doi.org/10.1088/0004-6256/149/3/91)
- 759 Plez, B. 2008, Physica Scripta Volume T, 133, 014003,  
760 doi: [10.1088/0031-8949/2008/T133/014003](https://doi.org/10.1088/0031-8949/2008/T133/014003)
- 761 Prantzos, N., Charbonnel, C., & Iliadis, C. 2007, A&A, 470,  
762 179, doi: [10.1051/0004-6361:20077205](https://doi.org/10.1051/0004-6361:20077205)
- 763 Renzini, A. 2008, Monthly Notices of the Royal  
764 Astronomical Society, 391, 354,  
765 doi: [10.1111/j.1365-2966.2008.13892.x](https://doi.org/10.1111/j.1365-2966.2008.13892.x)
- 766 Richer, H. B., Fahlman, G. G., Buonanno, R., et al. 1991,  
767 ApJ, 381, 147, doi: [10.1086/170637](https://doi.org/10.1086/170637)
- 768 Rousseeuw, P. J. 1987, Journal of Computational and  
769 Applied Mathematics, 20, 53,  
770 doi: [https://doi.org/10.1016/0377-0427\(87\)90125-7](https://doi.org/10.1016/0377-0427(87)90125-7)
- 771 Salaris, M., & Cassisi, S. 2005, Evolution of stars and  
772 stellar populations (John Wiley & Sons)
- 773 Sandage, A. R. 1953, AJ, 58, 61, doi: [10.1086/106822](https://doi.org/10.1086/106822)
- 774 Smith, G. H. 1987, Publications of the Astronomical  
775 Society of the Pacific, 99, 67, doi: [10.1086/131958](https://doi.org/10.1086/131958)
- 776 Sneden, C., Kraft, R. P., Prosser, C. F., & Langer, G. 1992,  
777 The Astronomical Journal, 104, 2121
- 778 Suntzeff, N. B., & Kraft, R. P. 1996, AJ, 111, 1913,  
779 doi: [10.1086/117930](https://doi.org/10.1086/117930)
- 780 Valle, G., Dell’Omodarme, M., & Tognelli, E. 2022, A&A,  
781 658, A141, doi: [10.1051/0004-6361/202142454](https://doi.org/10.1051/0004-6361/202142454)
- 782 van den Bergh, S. 2010, The Astronomical Journal, 140,  
783 1043, doi: [10.1088/0004-6256/140/4/1043](https://doi.org/10.1088/0004-6256/140/4/1043)
- 784 Ventura, P., & D’Antona, F. 2009, A&A, 499, 835,  
785 doi: [10.1051/0004-6361/200811139](https://doi.org/10.1051/0004-6361/200811139)
- 786 Ventura, P., D’Antona, F., Mazzitelli, I., & Gratton, R.  
787 2001, ApJL, 550, L65, doi: [10.1086/319496](https://doi.org/10.1086/319496)